View metadata, citation and similar papers at core.ac.uk

brought to you by CORE

provided by Missouri University of Science and Technology (Missouri S&T): Scholars' Mine

Missouri University of Science and Technology

Scholars' Mine

International Specialty Conference on Cold-Formed Steel Structures

(1975) - 3rd International Specialty Conference on Cold-Formed Steel Structures

Nov 24th, 12:00 AM

Buckling of Plates and Beam Sections under Stress Gradient

Shien T. Wang

Yei L. Tien

Follow this and additional works at: https://scholarsmine.mst.edu/isccss

 Part of the Structural Engineering Commons

Recommended Citation

Wang, Shien T. and Tien, Yei L., "Buckling of Plates and Beam Sections under Stress Gradient" (1975). *International Specialty Conference on Cold-Formed Steel Structures*. 1.
https://scholarsmine.mst.edu/isccss/3iccfss/3iccfss-session2/1

This Article - Conference proceedings is brought to you for free and open access by Scholars' Mine. It has been accepted for inclusion in International Specialty Conference on Cold-Formed Steel Structures by an authorized administrator of Scholars' Mine. This work is protected by U. S. Copyright Law. Unauthorized use including reproduction for redistribution requires the permission of the copyright holder. For more information, please contact scholarsmine@mst.edu.

BUCKLING OF PLATES AND BEAM SECTIONS UNDER STRESS GRADIENT

by

Shien T. Wang[1] and Yei L. Tien[2]

INTRODUCTION

The problem of local buckling of compression elements and members has been studied extensively in the past (4). However, most researchers only dealt with cases with idealized simple loading and edge conditions. In reality, the longitudinal edges of the compression flange of a flexural member are connected to and elastically restarined by, the web. In addition, as a result of moment gradient due to arbitrary loadings, the longitudinal compressive stress in the compression flange varies continuously along the length of the beam and is combined with the associated shearing and transverse stresses. These realistic loading and boundary conditions should be considered in the analysis.

In 1949, Libove, Ferdman, and Reusch (10) initiated a study on this general subject. They dealt with the elastic buckling of a simply supported flat rectangular plate with unequal uniform stresses applied at two transverse edges between which the stresses vary linearly. The difference between the compressive stresses at the two loaded edges is equilibrated by shearing stress along the longitudinal edges. Only recently, Chou and Gouwens (3) studied the elastic buckling of the compression flange of a wide flange beam subjected to a uniformly distributed load or a concentrated load at midspan. The elastic restraint along the joint was not considered in the above investigations.

---

[1] Assoc. Prof. of Civ. Engrg., Univ. of Kentucky, Lexington, Ky.

[2] Structural Analyst, Sargent and Lundy Engineers, Chicago, Ill., formerly, Grad. Asst., Univ. of Kentucky, Lexington, Ky.

The effects of elastic restraint along the edges on the buckling behavior of plates have been studied, however, by Johnson and Noel (8), Wittrick et.al. (25, 26, 27), Walker (15), and others. Although different stress combinations were considered, none considered the plates elastically restrained along the web-flange junction subjected to a stress gradient with shear effects.

On the other hand, work has also been carried out by researchers on local buckling of structural members as a whole. Bulson (1, 2) made a very inclusive review on the local instability of thin-walled sections subjected to uniform compression. Ghobarah and Tso (6) studied overall and local buckling of channel columns. Walker (16) investigated channel struts under an eccentric load. Rhodes and Harvey (12) studied the local buckling and post-local-buckling behavior of thin-walled channel beams under pure bending. A similar study on box girder was made by Grave-Smith (7). It is seen that the beam section subjected to a moment gradient has not yet been investigated.

Since the local buckling behavior of a component plate of a section or a beam as a whole subjected to realistic loading conditions is different from the idealized situations from which the current design data were derived, there is an apparent need in research on this subject. The purpose of this paper is to present a brief summary of a study on the buckling behavior of plates and beam sections subjected to varying compressive stress and shearing stress resultants derived from moment gradients due to arbitrary loadings. A numerical solution by the finite difference method with the aid of a digital computer is presented. Results are given for wide-flange and box beams under either a uniformly distributed load or a concentrated load at midspan.

STATEMENT OF THE PROBLEM

Fig. 1 shows an isotropic, elastic, rectangular plate with two transverse edges, x = 0, a, simply supported, one longitudinal edge along y = 0 elastically restrained, including two extremes, i.e. simply supported and clamped, and the other along y = b free or elastically restrained. The plate may represent the flange of a wide-flange section when free at y = b, or it can be considered as the flange of a box section or a web of any cross-section when elastically restrained along two longitudinal edges.

Using classical plate theory, the governing differential equation of a plate under in-plane forces can be written as

$$D\left(\frac{\partial^4 w}{\partial x^4} + 2\frac{\partial^4 w}{\partial x^2 \partial y^2} + \frac{\partial^4 w}{\partial y^4}\right) = N_x \frac{\partial^2 w}{\partial x^2} + N_y \frac{\partial^2 w}{\partial y^2}$$

$$+ 2N_{xy} \frac{\partial^2 w}{\partial x \partial y} - X\frac{\partial w}{\partial x} - Y\frac{\partial w}{\partial y} \qquad (1)$$

in which D = flexural rigidity of plate, i.e. $Et^3/12(1-\nu^2)$; w = deflection; N_x and N_y = membrane stress resultants (force/unit length) in x and y directions, respectively; N_{xy} = membrane shearing stress resultant; and ν = Poisson's ratio. The terms N_x, N_y and N_{xy} are positive as shown in Fig. 1. X and Y are body forces (force/unit area) in x and y directions, respectively, and are taken as zero in this investigation.

In the analysis, the slight curvature in the component plate of a beam section due to bending is neglected; the thickness, t, is assumed to be uniform; and the Poisson's ratio, ν, is taken as 0.25. It is also assumed that the edges x = 0, a, and y = 0 remain straight during

buckling. Same assumption applies to the edge y = b if elastically restrained.

Three loading conditions which are commonly encountered in practice are considered for both wide-flange and box beams:

Case 1 loading - The beam is loaded with a concentrated load at midspan, (Figs. 2(a) and 2(c)). The longitudinal stress resultant N_x in the compression flange varies linearly with x with a maximum value at midspan, and is combined with the associated shearing stresses (Figs. 3 and 5). The stress resultant distributions for the web and the bottom plate are also shown.

Case 2 loading - The beam is uniformly loaded (Figs. 2(b) and 2(d)). The longitudinal stress resultant N_x in the compression flange varies parabolically with x and is combined with the associated shearing stress resultant N_{xy} and the stress resultant N_y in the y direction (Figs. 4 and 6). The stress resultant distributions for the web and the bottom plate are also shown.

Case 3 loading - The plate or the beam section is subjected to axial uniform compression. This case is included so that the effect of stress gradient may be observed by comparing the results with those for loading cases 1 and 2.

The equations of stress resultants in the component plates of wide-flange and box beam sections subjected to the preceding loading conditions are derived based on the conventional beam theory by satisfying the following equations of equilibrium:

$$\frac{\partial N_x}{\partial x} + \frac{\partial N_{xy}}{\partial y} + X = 0 \tag{2}$$

$$\frac{\partial N_y}{\partial y} + \frac{\partial N_{xy}}{\partial x} + Y = 0 \tag{3}$$

The expressions of these stress resultants were obtained and presented in Ref. 13. The buckling of the compression flanges of wide flange and box beam sections will be presented first and then the buckling of beam sections will be discussed.

LOCAL BUCKLING OF PLATES

Boundary Conditions.--For an elastically restrained edge, the bending moments that appear during buckling along this edge are proportional at each point to the angle of rotation of the edge. Hence the corresponding boundary condition along the edge $y = 0$ is

$$\frac{\partial^2 w}{\partial y^2} + \nu \frac{\partial^2 w}{\partial x^2} = \epsilon \frac{\partial w}{\partial y} \tag{4}$$

Since along the joint edge of the plate $w = 0$, Eq. (4) becomes:

$$\frac{\partial^2 w}{\partial y^2} = \epsilon \frac{\partial w}{\partial y} \qquad \text{for } y = 0 \tag{5}$$

in which $\epsilon = -br/D(NR)$, an index from 0 to ∞; NR = the total number of rows of finite difference grids along y axis; and r = coefficient of fixity discussed in Ref. 14. In particular, when $\epsilon = 0, \infty$, the edge $y = 0$ is simply supported and fixed, respectively. When NR = 4, and $\epsilon = 0.5$, for example, the restraint is equivalent to $rb = 2$ as defined by Timoshenko and Gere (14). The values NR = 4 and $\epsilon = 2$ correspond to $rb = 8$.

If the edge $y = b$ is elastically restrained, the boundary condition is the same as Eq. (5). If $y = b$ is a free edge, the moment and shear along this edge vanish and leads to

$$\frac{\partial^2 w}{\partial y^2} + \nu \frac{\partial^2 w}{\partial x^2} = 0 \qquad \text{for } y = b \tag{6}$$

and

$$\frac{\partial^3 w}{\partial y^3} + (2 - \nu)\frac{\partial^3 w}{\partial x^2 \partial y} = 0 \quad \text{for } y = b \tag{7}$$

For simply supported edges along x = 0 and x = a, the boundary condition is

$$\frac{\partial^2 w}{\partial x^2} = 0 \qquad \text{for } x = 0, a \tag{8}$$

Difference Equations.--Using the finite difference method, the plate is divided by finite difference grids. Let NR denote the number of rows and NC denote the number of columns; the mesh length is h = a/NC and its width is k = b/NR. Eq. (1) for each nodal point is approximated by central differences. The approximation will involve twelve other points around the point. For points on or near boundaries, the fictitious points must be expressed in terms of deflections of interior nodal points by considering the boundary conditions.

Expressing Eq. 1 in the finite difference form together with the boundary conditions for each grid nodal point results in a set of simultaneous equations which can be written in matrix form as follows:

$$[L]\{w\} = K[M]\{w\} \tag{9}$$

in which [L] = a matrix containing the coefficients of biharmonic portion

of Eq.(1); [M] = a matrix containing the coefficients contributed by the in-plane stress resultants and body forces in Eq. (1); {w} = column matrix for nodal point deflections; and K = buckling coefficient in the following equation

$$(\overline{N}_x)_{cr} = K\frac{\pi^2 D}{b^2} \tag{10}$$

in which $\overline{N}_x$ = maximum value of stress resultant N_x; and $(\overline{N}_x)_{cr}$ = critical buckling stress resultant of $\overline{N}_x$.

Methods of Solution.--The solution for K is a general eigenvalue problem. It can be obtained by setting

$$\left| [L] - K [M] \right| = 0 \tag{11}$$

The difference equationsin Eq. (9) are generated row wise and column-wise from the assumed origin. The resulting matrix [L] may not be symmetric for a plate with a free edge along y = b, but the symmetry can still be achieved by carefully rearranging the sequence or formulating the difference equations (5). The matrix [L] is symmetric, however, when the edges y = 0 and y = b are elastically restrained. No attempt is made herein to set up a symmetric matrix [L], since matrix [M] is not symmetric for plates subjected to stress gradients using the approach introduced in Ref. 5. Following the coordinates of the nodal points, the programming of automatic generation of the finite difference operators appears to be straight foward since the bookkeeping of the coefficients in Eq. (9) is simple. No manual management of these input data is required.

The eigenvalue K is determined by a determinate search technique. The approach is based on a linear interpolation when two consecutively calculated K values have changed sign of the determinant. In this case, the initial value of K and the step size must be specified. The rate of convergence depends substantially upon the size of increment used in each step. In general, the incrementing step size should be kept small enough in order to ensure that the smallest eigenvalue is obtained. Additional considerations were discussed in Ref. 13.

In evaluating the determinant, a value of K is assumed. Using Gaussian elimination, the matrix is transformed into an upper triangular form. In every step of Gaussian elimination, the pivoting elements are formed and the equations are rearranged so that the diagonal elements dominate. The product of the diagonal elements of this transformed matrix is equal to the determinant. After determining the eigenvalue K, by back substition, one can obtain the corresponding eigenvector. The largest element of the eigenvector is found and the eigenvector is then normalized by dividing the elements by this largest element.

A solution scheme based on the Trace Theorem (9) is also employed. The Trace Theorem provides a Newton-Raphson correction which is of second order and therefore can speed up the rate of convergence. It has been found that the solution scheme based on the Trace Theorem reduces the number of iterations considerably. However, the Trace Theorem requires the inverse of the matrix and the cost is comparable to that of the determinate search method for the cases considered. This approach does not require a prespecified increment size for the solution. The results obtained by both approaches

are practically identical.

Some results obtained by the above procedures have been verified by using an eigenvalue subroutine EECM from NASA (11). The NASA program utilizes the QR algorithm, Hessenberg matrix and the deflation procedure (23). EECM processes all eigenvalues and eigenvectors, including complex numbers, for both symmetric and nonsymmetric matrices. It requires more storage and costs more to run than the program developed herein.

Comparison with Existing Solutions.--A computer program following the preceding solution schemes based on the determinate search technique and the Trace Theorem outlined was developed (13). The boundary conditions for the plate may be simply supported, fixed or elastically restrained. In addition, the longitudinal edge along y = b may be free. Arbitrary loading conditions can be specified using the derived associated stress resultants. By considering the compatibility conditions along the joints of a section, the program was used to investigate the local instability problems of beam sections.

Using the developed program, numerical results were obtained for two cases and are compared with the solutions by the previous investigators as shown in Fig. 7.

In Fig. 7(a), Timoshenko and Gere (14) treated a uniformly compressed plate simply supported along two transverse edges, x = 0, a. The longitudinal edge y = 0 is elastically restrained ranging from simply supported to fixed condition, while edge y = b is free. For finite difference solutions, the width of the plate was divided into four equal divisions for the square finite difference grids.

Libove et. al. (10) investigated the simply supported plate under

a compressive stress that varies linearly from one transverse edge to the other, the difference in stress being equilibrated by uniform shears along the longitudinal edges as shown in Fig. 7(b). The minimum and maximum stresses at the transverse edges were defined as $(N_x)_{min}$ and $(N_x)_{max}$, respectively. The ratio of $(N_x)_{min}/(N_x)_{max}$ was 0.2. For finite difference solutions, the width of the plate was divided into five equal divisions for the square finite difference grids.

It is seen that the computed results agree closely with those obtained by the previous investigators.

Local Buckling of Compression Flange of Wide Flange Beams. --

Case 1 Loading: The distribution of stress resultants for the compression flange of a wide flange beam subjected to a concentrated load at midspan is shown in Fig. 3(a). The buckling coefficients are plotted in Fig. 8 as a function of aspect ratios (length/width) in variation with the elastic restraint, ϵ, along the longitudinal edge $y = 0$. The aspect ratio ranges from 1.4 to 9. Although the aspect ratio of a beam may be twice this value, the envelope of the buckling curves flattens out rapidly. For finite difference grids, the plate was divided into square meshes when the aspect ratio was less than 3.75; for higher ratios, rectangular meshes were used. The ratio between the grid spacings in the x and y directions varied from 1 to 4. The number of divisions on the x direction varied from 5 to 15, and that in the y direction ranged from 4 to 6. Three values, 0, 2, and ∞ for elastic restraint, ϵ, along $y = 0$ were considered. The buckling coefficients for plates subjected to uniform compression without any shear effects (case 3 loading) are also plotted in the same figure

for comparison. An excellent agreement is obtained between the computed results and those by Chou and Gouwens (3) for the case $\varepsilon = 0$.

The buckling coefficient of the plate with an aspect ratio of 9, for example, is 0.7 when $\varepsilon = 0$ and 1.45 when $\varepsilon = \omega$ along the edge $y = 0$. For a real beam flange with the same aspect ratio, the buckling coefficient should be within these limits. From the figure, it is seen that the computed buckling coefficients are much higher than that of a uniformly compressed plate, especially for plates with small aspect ratios.

Some typical buckling mode shapes are shown in Fig. 9, where the curves depict the buckling shapes along the free edge and those in the transverse direction close to the middle of the plates. For simply supported case, as shown in fig. 9(a), the buckling mode deviates from the standard sine wave. The maximum amplitudes of the buckling wave are shifted and squeezed towards the midspan of the plate. This phenomenon is more evident for longer plates with large aspect ratios (Fig. 9(b)). In this case, the largest amplitudes of the buckling wave occur in the central portion of the plate while the wave close to two ends of the plate flattens out remarkably (20). It is also interesting to note that the wave length for the buckling mode is shorter in the central portion than that in the end regions. The buckling shapes in the transverse direction are close to straight lines when the edge $y = 0$ is simply supported; but deviated from straight line slightly when the edge $y = 0$ is elastically restrained.

Casd 2 Loading: The distribution of stress resultants for the compression flange of a wide flange beam subjected to a uniformly

distributed load is shown in Fig. 4(a). The buckling coefficients are plotted against the aspect ratio for various elastic restraints along the edge y = 0 in Fig. 8. The aspect ratio ranges from 1 to 9. The arrangements for the finite difference grids and the boundary conditions were the same as those used in the preceding case. Again, the results for the case $\varepsilon = 0$ check closely with those obtained by Chou and Gouwens (3).

The computed buckling coefficients are again higher than those of a uniformly compressed plate, especially for plates with small aspect ratios. But, the difference is smaller than that of case 1 loading. The effects of stress gradients on mode shapes are similar to those of case 1 loading.

Local Buckling of Compression Flange of Box Beams.--For a box beam subjected to cases 1 and 2 loading, the stress resultant distributions in the compression flange are shown in Figs. 5(a) and 6(a), respectively. The longitudinal edges of the compression flange are elastically restrained by the webs. The aspect ratio considered ranged from 1 to 9. For finite difference grids, the plate was divided into four rows of nodal points in the transverse direction; by virtue of summetry,only two rows of nodal points had to be considered in the finite difference formulation. The number of division in the x direction varied from 5 to 15 depending upon the aspect ratio of the plate. Both square and rectangular meshes were used, the ratio of mesh spacing in x - direction to that in the y - direction varying from 1 to 3. The computed buckling coefficients are plotted as functions of the aspect ratio of the plate in Fig. 10. Only results for plates with all edges simply supported are presented.

Under case 1 loading, the buckling coefficient for the plate with aspect ratio of 9, for example, is 4.17 which is only slightly larger than 4 of a uniformly compressed plate. If the box beam is rather short, the effects of shearing stress is significant and the computed buckling coefficients are much larger than that of a uniformly compressed plate without stress gradients.

Under case 2 loading, in deriving the expression for N_y, it was assumed that $N_y = 0$ along the longitudinal edges $y = 0$ and b. The same assumption was made in an earlier study by Winter (24). For a plate with a small aspect ratio, the buckling coefficient may be less than 4. The assumption of the stress condition of $N_y = 0$ along two longitudinal edges is partially responsible for this weakening effect. For a long plate, however, the influence of N_y becomes insignificant. Therefore, the effects caused by the assumption concerning the distribution of N_y are also likely to be negligible for long plates.

Fig. 11 shows the typical buckling mode of the compression flange of a box beam. Similar to the compression flange of a wide flange section, the maximum amplitude of the buckling wave occurs in the central portion of the plate, and the buckling wave flattens out rapidly towards the ends (20). Again, the wave length is shorter in the central region than that close to the two ends.

LOCAL BUCKLING OF BEAM SECTIONS

Fig. 12 shows the general form of a section with different geometries and boundary conditions representing several kinds of sections. If the edges $y_1 = b_1$, $y_3 = b_3$, $y_4 = b_4$ and $y_5 = b_5$ are free, it represents a wide-flange section. If the edges $y_1 = b_1$, and $y_3 = b_3$ are free, and $b_4 = b_5 = 0$, it represents a channel section. If the edges $y_1 = b_1$, $y_3 = b_3$ are in the plane of symmetry, and $b_4 = b_5 = 0$, it stands

for the left half of a box section. By virtue of symmetry or antisymmetry of the corss-section, only three plates, i.e. No. 1, 2 and 3 are treated. In most studies, symmetry is taken about the horizontal plane crossing the middle of plate No. 2. However, for beams subjected to moments, lower half of plate No. 2 and plates No. 3 and 5 are in tension, thus this symmetry no longer exists. On the other hand, symmetry or anti-symmetry about the plane of plate No. 2 holds for the situation considered and is, therefore, adopted in this investigation.

Boundary Conditions.-- For a number of long plates joined along longitudinal edges to form a structural member, the following boundary conditions are normally applied when local buckling occurs:

(i) The common edges of component plates remain straight. The primary failure of the entire structure does not occur before the occurrence of local buckling.

(ii) The plates are rigidly joined along the edges. This implies that all the plates which meet at one edge rotate through the same angle when the cross-section distorts.

(iii) The moment is in equilibrium at the junction of plates.

Consider the nth component plate with width b_n and thickness t_n. The subscript n denotes the nth component plate. The edge $y_n = 0$ remains straight, and the original angle between the nth and (n + 1)th plate is maintained. Therefore,

$$[w_n = 0]_{y_n=0} \tag{12}$$

and

$$\left[\left(\frac{\partial w}{\partial y}\right)_n\right]_{y_n=0} - \left[\left(\frac{\partial w}{\partial y}\right)_{n+1}\right]_{y_n=0} = 0 \tag{13}$$

There is also equilibrium of moments about the common edge of all plates, so that

$$\sum \left[-D_n\left(\frac{\partial^2 w}{\partial y^2} + \nu \frac{\partial w}{\partial y^2}\right)\right]_{n \; y_n=0} = 0 \tag{14}$$

in which D_n = flexural rigidity of nth component plate.

Along the free edge of the plate, zero moment and zero shear give two boundary conditions as follows:

$$\left[D_n \left(\frac{\partial^2 w}{\partial y^2} + \nu \frac{\partial^2 w}{\partial x^2}\right)\right]_{n \; y_n=0} = 0 \tag{15}$$

and

$$\left[D_n \left(\frac{\partial^3 w}{\partial y^3} + (2 - \nu) \frac{\partial^3 w}{\partial x^2 \partial y}\right)\right]_{n \; y_n=0} = 0 \tag{16}$$

For a simply supported beam, there is no moment at the transverse edge, x = 0, a, of the plate, i.e.

$$D_n \left[\frac{\partial^2 w}{\partial x^2} + \nu \frac{\partial^2 w}{\partial y^2}\right]_n = 0 \tag{17}$$

Difference Equations and Method of Solution.--In the analysis, each plate is discretized by rectangular finite difference grids. The mesh size in the longitudinal direction remains constant for every plate, while in the transverse direction the mesh size can be different for each plate under consideration. For each nodal point, Eq. (1) is then approximated by central differences. Using the preceding boundary conditions, the deflections of fictitious points lying outside

the plate are converted in terms of the interior nodal points and the related flexural rigidities, D's, and the mesh widths k's of the component plates. Boundary conditions in the finite difference form for the free and simply supported edges are the same as those for plates discussed earlier.

Expressing Eq. (1) in finite difference form together with the boundary conditions for each nodal point in the sequence of plates No. 1, 2 and 3 (see Fig. 12) and in each plate following the order as described earlier for plates, a set of simultaneous equations are obtained, which can be written as Eq. (9). The value for K can be obtained from Eq. (11) using the same solution procedures described earlier for plates. The eigenvalue is the buckling coefficient for the section, which can be expressed in terms of either the dimensions and elastic material properties of the compression flange or that of the web. If the buckling stress of the section is referred to the compression flange, the following equation is obtained

$$\sigma_{cr} = \frac{K_f \pi^2 D_f}{b_f^2 t_f} \tag{18}$$

in which $\sigma_{cr} = (\overline{N}_x)_{cr}/t_f$; f = subscript referring to flange; and K_f = buckling coefficient expressed in terms of properties of flange.

Comparison with Existing Solutions.--The computer program prepared can be applied to plain channels, box and wide-flange sections directly under general loading conditions. With slight modifications, the programs can be used for other sections.

Considering the wide flange section subjected to uniform compression (Fig. 13(a)), each component plate was discretized by five rows and five columns of finite difference grids. The computed results

are found to be in excellent agreement with those by Bulson (1).

When a channel section column loaded eccentrically, the stress distribution is a combination of compressive and bending stresses as shown in Fig. 13(b). The plain channel section with $a/b_w = 1$ and $t_w/t_f = 1$ simply supported at two ends and free at the bottom edge of the flanges under the stress distribution shown was considered. Again, each plate was discretized by five rows and five columns of finite difference grids. The results show remarkable agreement with Walker's solution (15).

In Fig. 13(c), a simply supported concentrically loaded box column was considered. By virtue of symmetry, only half section was dealt with. Top and bottom flanges were discretized by two rows and four columns of finite difference nodal points inside the plate and the web was discretized by four rows and four columns of finite difference nodal points. Two cases of Bulson's results (1) were analyzed; one corresponds to $a/b_f = 1.0$, $b_w/b_f = 1.0$, $t_w/t_f = 1.0$ and the other corresponds to $a/b_f = 1.3$, $b_w/b_f = 1.5$, $t_w/t_f = 1.0$. The computed results agree with Bulson fairly well. The accuracy can always be improved by using finer mesh size if necessary.

Local Buckling of Wide Flange Beams.--For a wide flange beam subjected to cases 1 and 2 loading, the distributions of stress resultants in the component plates are shown in Figs. 3 and 4. For finite difference grids, four equal divisions in the transverse direction of the top and bottom plates (half) were used, while a variety of equal divisions in the longitudinal direction were used depending on the a/b_f ratio. For the web, the plate was divided into five equal

divisions in the transverse direction while in the longitudinal direction the number of division was kept the same as that of the flanges.

Under case 1 loading, the buckling coefficients for wide-flange sections of various geometry and length are given in Fig. 14(a). In the same figure, the curves of buckling coefficients for the top flange with simply supported or clamped longitudinal edge (Fig. 8) are also presented. The buckling coefficients of the beam sections are slightly higher than the case for plates with simply supported edge under the same loading condition. For buckling modes, the compression flange has the largest buckling amplitude; the tension flange buckles only slightly; and the upper half of the web buckles with larger amplitude than the lower half.

Under case 2 loading, the buckling coefficients are shown in Fig. 14(b) along with the curves for compression flange with a simply supported or clamped edge under the same loading (Fig. 8). For rather long beams, the compression flange limits the buckling strength. On the other hand, for shorter beams or longer beams but with comparatively deep webs, the buckling coefficients are lower than those based on compression flange. This is due to the interaction of local buckling in the web and in the compression flange for the overall section under consideration. Comparing Figs. 14(a) and 14(b), it is seen that the buckling behavior for the same section under loading cases 1 and 2 is different. It should be noted that for wide-flange sections subjected to case 1 loading, stress resultant N_y is not present; however, under loading case 2, the stress resultant N_y does exist in the web. The presence of N_y in the web weakens the section and reduces the buckling strength of the overall section especially when the web is deep. In this case the web will most likely buckle locally

prior to flange buckling. This accounts for the low buckling strength for the short and deeper sections. For those sections, the maximum buckling amplitude occurs in the web.

Local Buckling of Box Beams.--For a box beam subjected to cases 1 and 2 loading, the distributions of stress resultants in the component plates are shown in Figs. 5 and 6. In the analysis, only the left half section was considered by virtue of symmetry. For finite difference grids, the top and bottom plates were divided into four rows and four to ten columns depending on the ratio of a/b_f. The web was divided into four rows and kept same number of columns as in flanges.

Under loading case 1, the buckling coefficients versus the ratio of span length to the flange width are given in Fig. 15(a). The thicknesses of flanges and web were kept the same. The buckling curve for the compression flange simply supported along the longitudinal edges subjected to the same loading condition (Fig. 10) is also presented in the same figure for comparison. The results show that the buckling coefficients of the integral sections are somewhat higher than those for compression flange alone with simply supported longitudinal edges under the same loading condition. Similar to the wide-flange sections, the compression flange has the largest buckling amplitude; the tension flange waves only slightly. The amplitude of the buckling wave in the central region along the beam length is much larger than that in the end portions and the wave length in the central region is shorter than that close to the two ends. This phenomenon was also observed for wide-flange beams and for the compression flange plate alone.

Under case 2 loading, the buckling coefficients are shown in

Fig. 15(b) along with the buckling curve for the compression flange with simply supported edges subjected to the same loading (Fig. 10). Similar to wide flange section, the compression flange limits the strength of the section for long beams. In this case, the buckling coefficients are higher than those based on the simply supported compression flange alone. For short beams or long deep beams, the overall buckling stress of the integral section governs due to the interaction of flange and web buckling. In this case, the buckling is most likely to initiate in the web, expecially for sections with large depth to flange width ratios, i.e. b_w/b_f.

CONCLUSIONS

The primary conclusions which can be drawn from this study are as follows:

1. The developed computer program is capable of solving buckling problems of plates with various boundary conditions and wide-flange, plain channel and box sections under various loading conditions. The program can also be used for other cases. The techniques used, based on the determinant search approach or the Trace Theorem, proved to be efficient in solving eigenvalues of symmetric as well as nonsymmetric matrices.

2. For long plates, the effects of stress gradient (longitudinal) on the buckling coefficients are not significant. The buckling is governed by the maximum longitudinal compressive stress at mid-span. Effects resulting from other factors such as shear, transverse stress and pattern of distribution are also insignificant.

3. For short plates, the effects of stress gradient on the

buckling coefficients are evident when the plates are subjected to stress resultants due to case 2 loading (uniform load) and are even more evident under case 1 loading (concentrated load at mid-span).

4. In general, plates under case 1 loading give the highest buckling coefficients, while the plates under case 2 loading give slightly higher buckling coefficients than those under case 3 loading (uniform compression).

5. The effects of elastic restraint along longitudinal edges on the buckling coefficients are greater when the aspect ratio is large. On the other hand, the stress gradient has a greater effect when the longitudinal edges are simply supported than when they are completely restrained.

6. Due to the effects of stress gradient, the buckling wave pattern is not uniform. The amplitude of the buckling wave is maximum in the central region of the plate and the wave length in the central region is shorter than that close to the two ends.

7. In the initial post-buckling range of a buckled plate, the waving pattern will follow the buckling modes. Since the effective width of the buckled plate has a close relationship to the waving amplitude, it may be concluded that the effective width of the compression flange would vary along the length of the beam depending upon the moment gradient involved (17, 18, 19, 20, 21, 22).

8. Under case 1 loading, the buckling strength of the beams considered in this investigation is governed by the compression flange. Under case 2 loading, local buckling may be initiated in the web, especially for the short deep beams considered. The interaction of web and flange buckling must be considered.

9. Since the expressions of stress resultants used in the buckling analysis are derived based on the conventional beam theory, additional studies are necessary for cases with shear lag effects. The general method developed, however, is applicable in those cases.

APPENDIX I. - REFERENCES

1. Bulson, P.S., "Local Stability and Strength of Structural Sections," Thin-Walled Structures, edited by A.H. Chilver, John Wiley and Sons, Inc., 1967.

2. Bulson, P.S., The Stability of Flat Plates, American Elsevier Publishing Company, Inc., New York, 1969, pp. 295-371.

3. Chu, K.H., and Gouwens, A.J., "Elastic Buckling of Beam Flange Plates," Journal of Engineering Mechanics Division, ASCE, No. EM4, Vol. 97, August, 1971, pp. 1329-1336.

4. Column Research Council of Japan, Handbook of Structural Stability, 1971.

5. Gali, A., and Neville, A.M., Structural Analysis--A Unified Classical and Matrix Approach, Intext Educational Publishers, 1972, pp. 500-502.

6. Ghobarah, A.H., and Tso, W.K., "Overall and Local Buckling of Channel Columns," Journal of the Engineering Mechanics Division, ASCE, No. EM2, April, 1969, pp. 447-462.

7. Graves-Smith, T.R., "The Local Buckling of Box Girders, Under Bending Stress," International Journal of Mechanical Sciences, Vol. 11, July-December, 1969, pp. 603-612.

8. Johnson, J.H., and Noel, R.G., "Critical Bending for Flat Rectangular Plates Supported Along All Edges and Elastically Restrained Against Rotation Along the Unloaded Compression Edge," Journal of the Aeronautical Sciences, August, 1953, pp. 535-540.

9. Lancaster, P., Lambda Matrices and Vibrating Systems, Pengamon Press, 1966, pp. 82-85.

10. Libove, C., Ferdman, S., and Reusch, J.J., "Elastic Buckling of a Simply Supported Plate Under a Compressive Stress that Varies Linearly in the Direction of Loading," NACA, Technical Note 1891, June, 1949.

11. NASA, Subroutine EECM, Computer Programming Manual, Vol. I, Section F2.7, Langley Research Center, March, 1970.

12. Rhodes, J., and Harvey, J.M., "The Local Buckling and Post-Local-Buckling Behavior of Thin-Walled Beams," Journal of Aeronautical Quarterly, 1971, pp. 363-388.

13. Tien, Y.L., "Local Buckling of Plates and Sections of Flexural Members Under Stress Gradients," a dissertation submitted in partial fulfillment of the requirements for the degree of Doctor of Philosophy at the University of Kentucky, Lexington, Kentucky, April, 1975.

14. Timoshenko, S. P., and Gere, J. M., Theory of Elastic Stability, McGraw-Hill Book Company, Inc., New York, 1964.

15. Walker, A. C., "Local Instability in Plates and Channel Struts," Journal of the Structural Division, ASCE, Vol. 92, No. ST3, June, 1966, pp. 39-55.

16. Walker, A. C., "Maximum Loads for Eccentrically Loaded Thin-Walled Channel Struts," IABSE Publications, International Association for Bridge and Structural Engineering, 1968, pp. 169-180.

17. Wang, S. T., and Tien, Y. L., "Post-Local Buckling Behavior of Thin-Walled Columns," Proceedings of the Second Specialty Conference on Cold-Formed Steel Structures," St. Louis, Missouri, 1973, pp. 53-81.

18. Wang, S. T., and Yeh, S. S., "Post-Local-Buckling Behavior of Continuous Beams," Journal of the Structural Division, ASCE, Vol. 100, ST6, June, 1974, pp. 1169-1187.

19. Wang, S. T., and Jsa, S. T., "Stiffness Analysis of Locally Buckled Thin-Walled Continuous Beams," International Journal of Computers and Structures, Vol. 5, No. 1, April, 1975, pp. 81-93.

20. Wang, S. T., "Post-Buckling Behavior of Continuous Box Girders," Proceedings of the ASCE Specialty Conference on Metal Bridges, St. Louis, Missouri, 1974, pp. 173-200.

21. Wang, S. T., and Jsa, S. T., "Post-Local Buckling Behavior of Multistory Frames," Proceedings of the Symposium on Planning, Design, and Construction of Tall Buildings, Nashville, Tennessee, November, 1974, pp. 459-476.

22. Wang, S. T., "Nonlinear Analysis of Locally Buckled Thin-Walled Structures," Proceedings of the First International Conference on Computational Methods in Nonlinear Mechanics, Austin, Texas, September, 1974, pp. 809-818.

23. Wilkinson, J. H., The Algebraic Eigenvalue Problem, Oxford: Clarendon Press, England, 1965.

24. Winter, G., "Stress Distribution in an Equivalent Width of Flanges of Wide, Thin-Walled Steel Beams," Ph. D. Dissertation, Cornell University, Ithaca, New York, 1940, (also NACA Technical Note No. 784, 1940).

25. Wittrick, W. H., and Curzon, P. L. V., "Local Buckling of Long Polygonal Tubes in Combined Compression and Torsion," International Journal of the Mechanical Sciences, Vol. 10, 1968, pp. 849-857.

26. Wittrick, W. H., and Curzon, P. L. V., "Stability Function of Thin-Flat-Walled Structures with the Walls in Combined Shear and and Compression," Aeronautical Quarterly, Vol. 19, 1968, pp. 327-351.

27. Wittrick, W. H., and Curzon, P. L. V., "Nodal Lines for Long Plates in Combined Shear and Compression with Sinusoidal Edge Rotations," Aeronautical Quarterly, 1969, pp. 1-16.

APPENDIX II. - NOTATION

The following symbols are used in this paper:

a, b = length and width of plate in x, y directions, respectively;

b_n = width of nth component plate in y direction;

D = flexural rigidity of plate;

E = modulus of elasticity;

f = subscript referring to flange;

h = a/NC, finite difference mesh length;

K = buckling coefficient;

K_f = buckling coefficient expressed in terms of properties of flange;

$(K_f)_{min}$ = minimum K_f as defined in Ref. 1;

K_w = buckling coefficient expressed in terms of properties of web;

$(K_w)_{min}$ = minimum K_w as defined in Ref. 1;

k = b/NR, finite difference mesh width;

$[L]$ = matrix containing coefficients of biharmonic portion;

$[M]$ = matrix containing coefficients contributed by in plane stress resultants and body forces;

N_x, N_y = membrane stress resultants (force/unit length) in x and y directions, respectively;

$(N_x)_{max}$, $(N_x)_{min}$ = maximum and minimum N_x along two transverse edges as defined in Ref. 10;

$\overline{N}_x$ = maximum value of stress resultant N_x;

$(\overline{N}_x)_{cr}$ = critical buckling stress resultant of $\overline{N}_x$;

N_{xy} = membrane shearing stress resultant;

NC = total number of columns of finite difference grids along x axis;

NR = total number of rows of finite difference grids along y axis;

n = subscript referring to nth component plate;

r = coefficient of fixity defined in Ref. 14;

t_n = thickness of nth component plate;

$\{w\}$ = columns matrix for nodal point deflections;

w = deflection; subscript referring to web;

X, Y = body forces (force/unit area) in x and y directions, respectively;

x, y, z = coordinates;

x_n, y_n, z_n = coordinates of nth component plate;

ν = Poisson's ratio;

ϵ = $-br/D(NR)$, index from 0 to ∞; and

σ_{cr} = $(\overline{N}_x)_{cr}/t_f$, buckling stress.

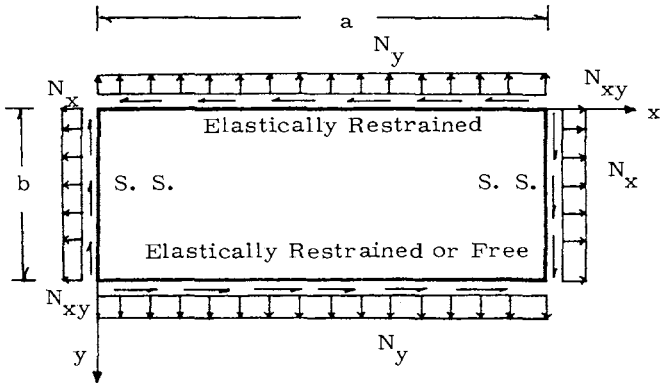

FIG. 1. - RECTANGULAR PLATE

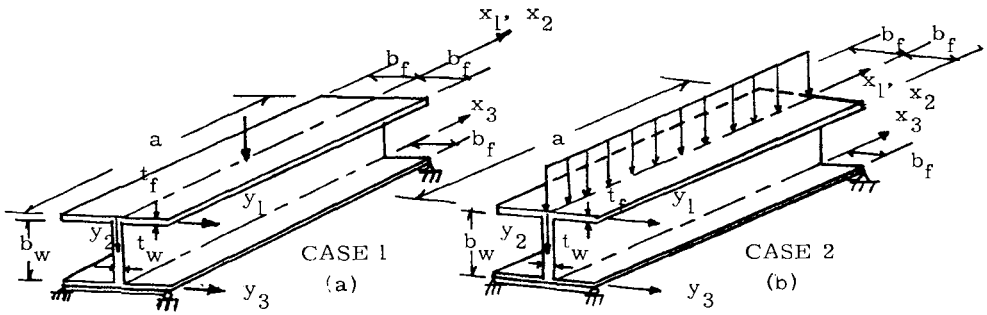

LOADING CASES FOR WIDE-FLANGE BEAMS

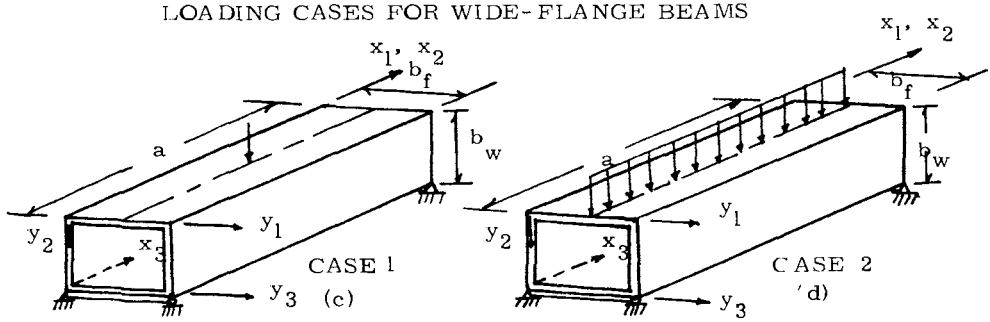

LOADING CASES FOR BOX BEAMS

FIG. 2. - LOADING CASES AND BEAM SECTIONS

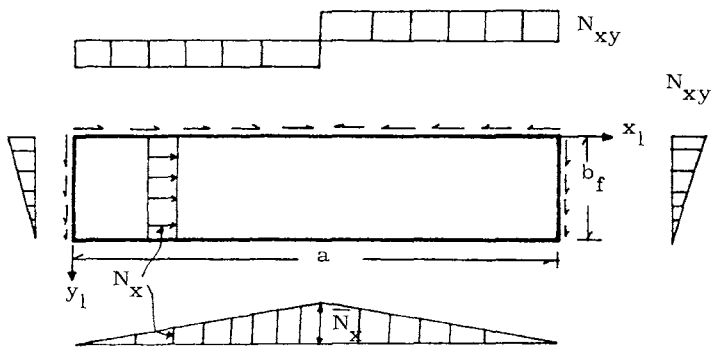

(a) Top Flange

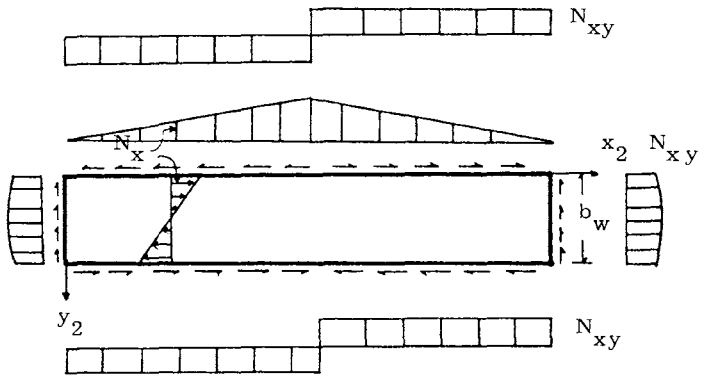

(b) Web

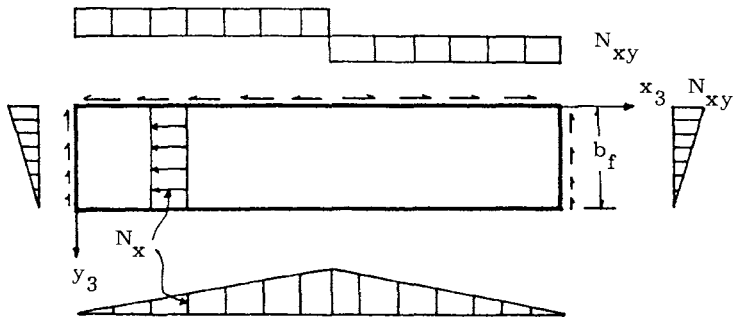

(c) Bottom Flange

FIG. 3. - STRESS RESULTANT DISTRIBUTIONS - WIDE-FLANGE BEAM SUBJECTED TO CASE 1 LOADING

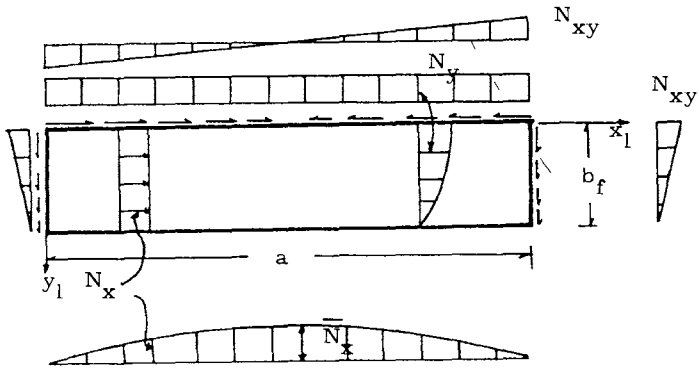

(a) Top Flange

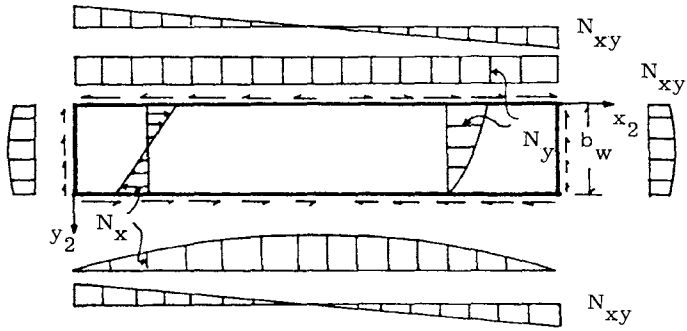

(b) Web

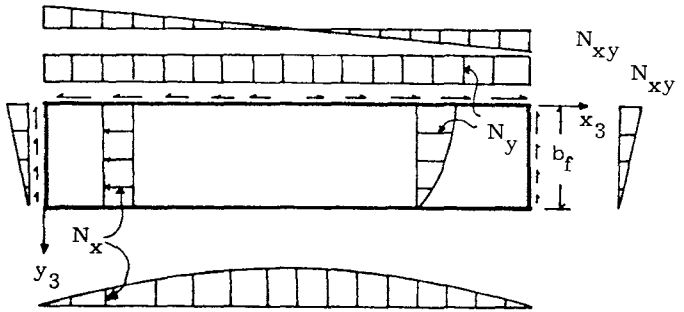

(c) Bottom Flange

FIG. 4. - STRESS RESULTANT DISTRIBUTIONS - WIDE-FLANGE BEAM SUBJECTED TO CASE 2 LOADING

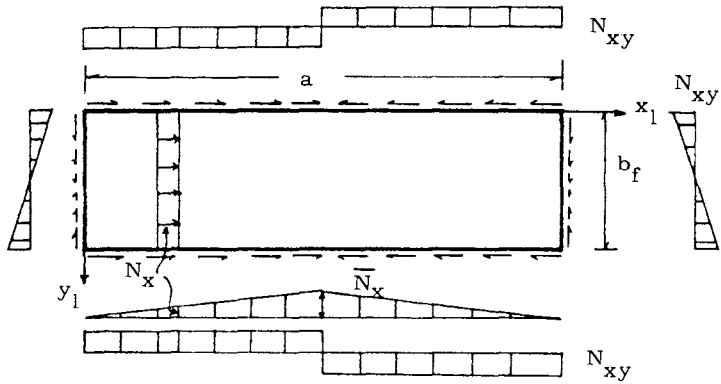

(a) Top Flange

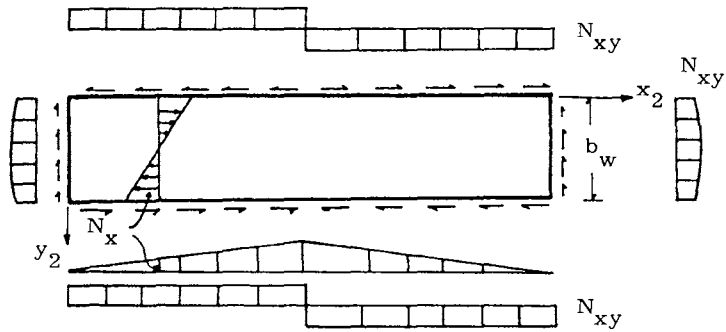

(b) Web

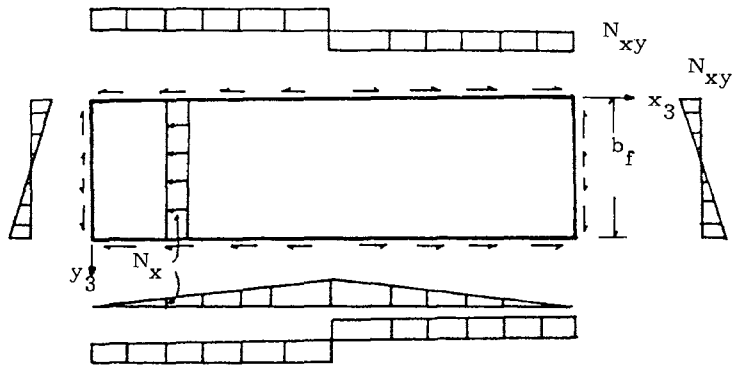

(c) Bottom Flange

FIG. 5. - STRESS RESULTANT DISTRIBUTIONS - BOX BEAM SUBJECTED TO CASE 1 LOADING

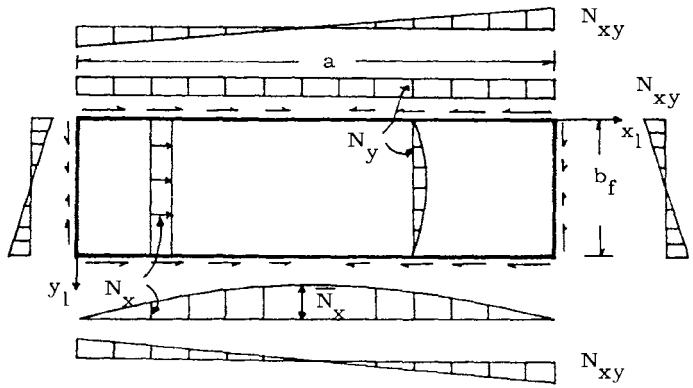

(a) Top Flange

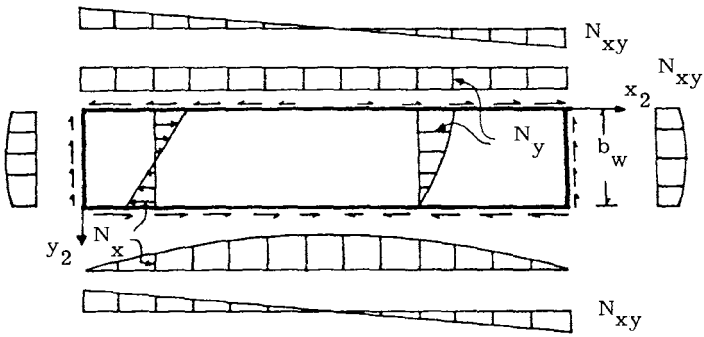

(b) Web

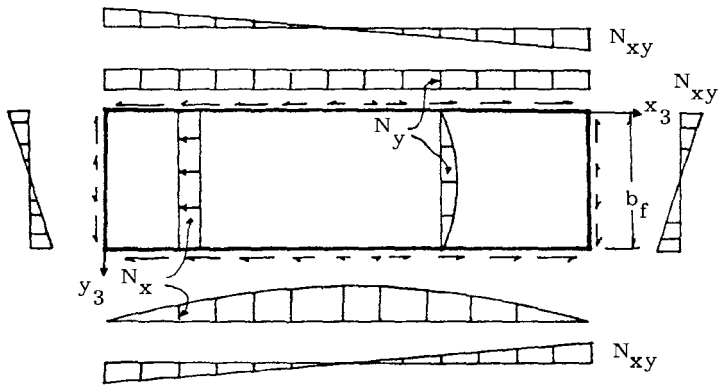

(c) Bottom Flange

FIG. 6. - STRESS RESULTANT DISTRIBUTIONS - BOX BEAM SUBJECTED TO CASE 2 LOADING

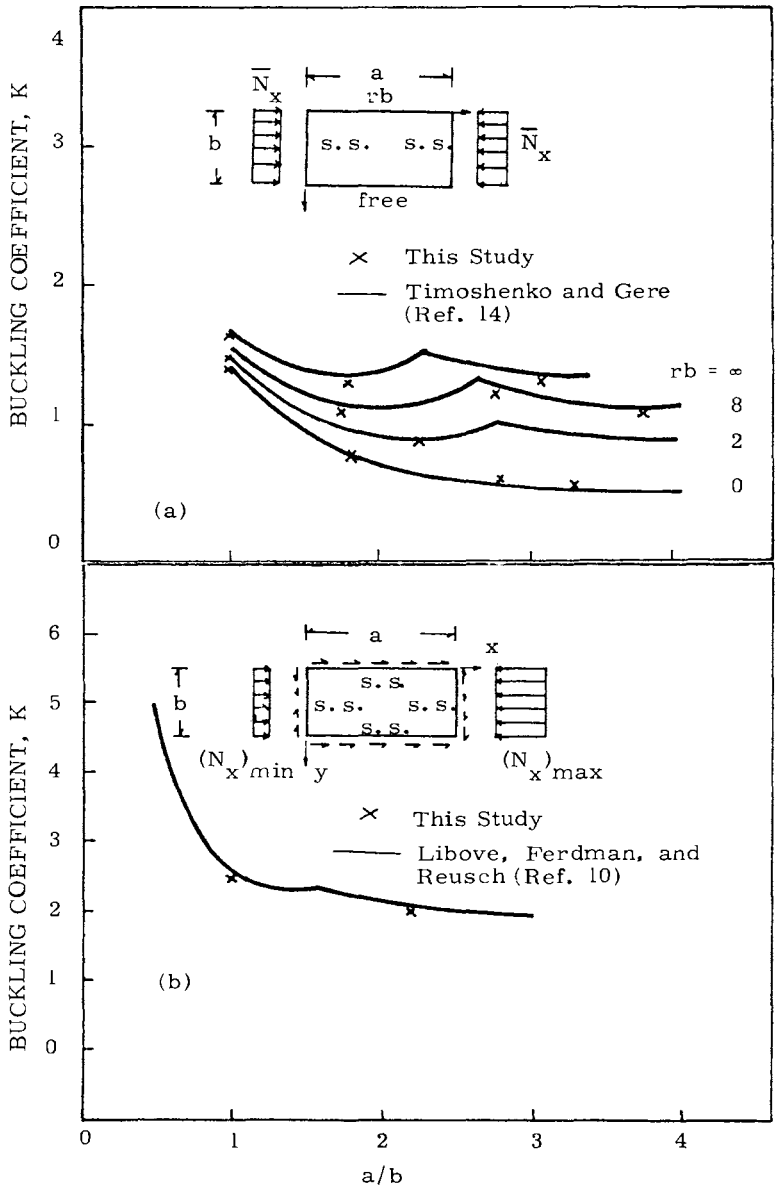

FIG. 7. - COMPARISON OF SOLUTIONS - BUCKLING OF PLATES

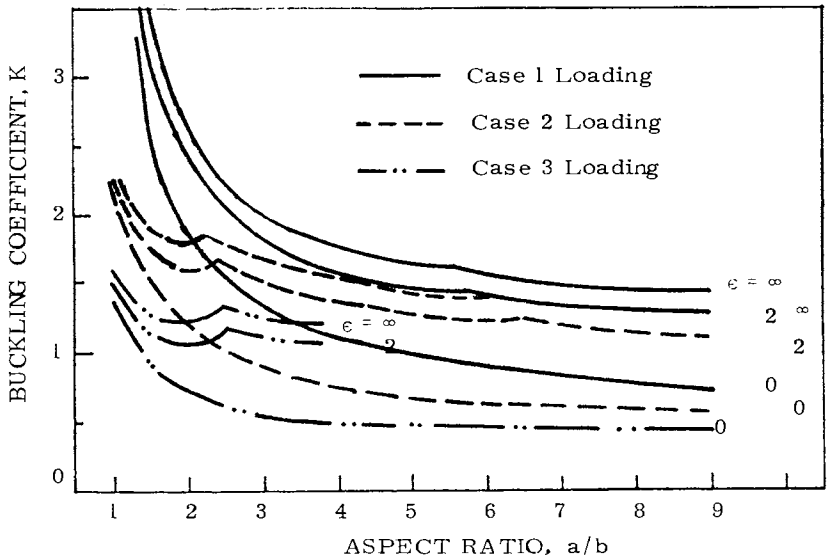

FIG. 8. - BUCKLING COEFFICIENTS OF COMPRESSION FLANGE OF WIDE-FLANGE BEAMS UNDER VARIOUS LOADING CASES

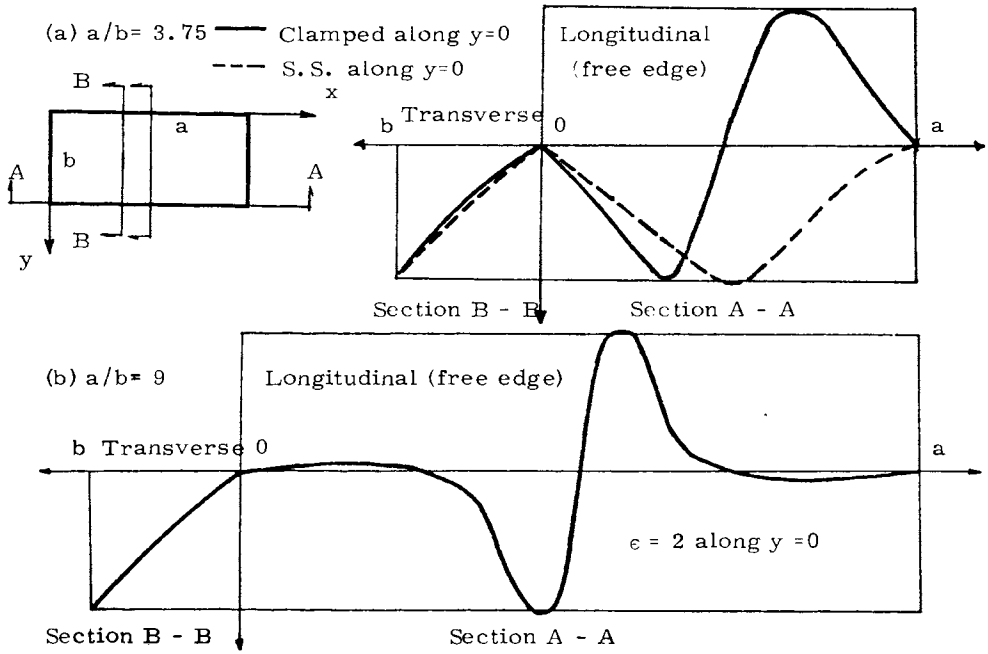

FIG. 9. - BUCKLING MODES FOR COMPRESSION FLANGE OF WIDE-FLANGE BEAM UNDER CASE 1 LOADING

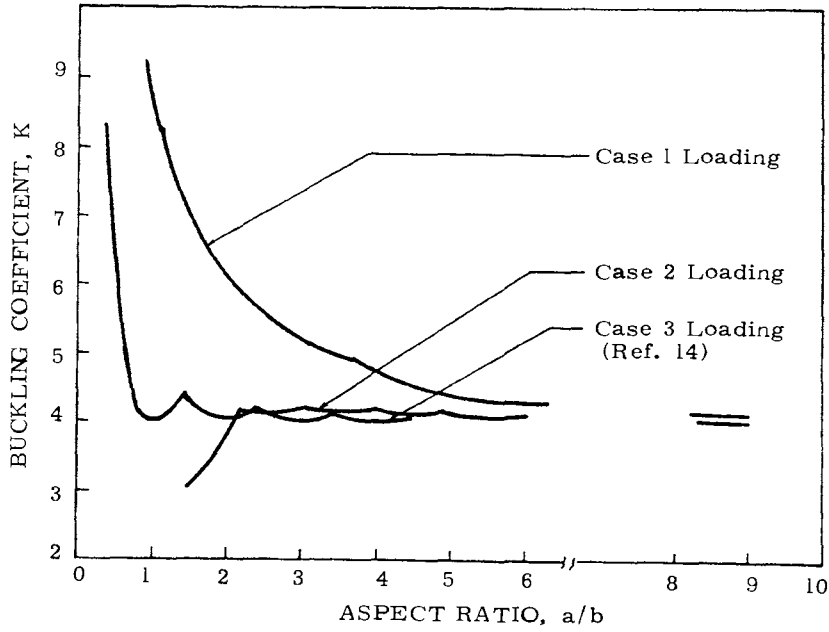

FIG. 10. - BUCKLING COEFFICIENTS OF COMPRESSION FLANGE (S. S. ALONG y = 0, b) OF BOX BEAMS UNDER VARIOUS LOADING CASES

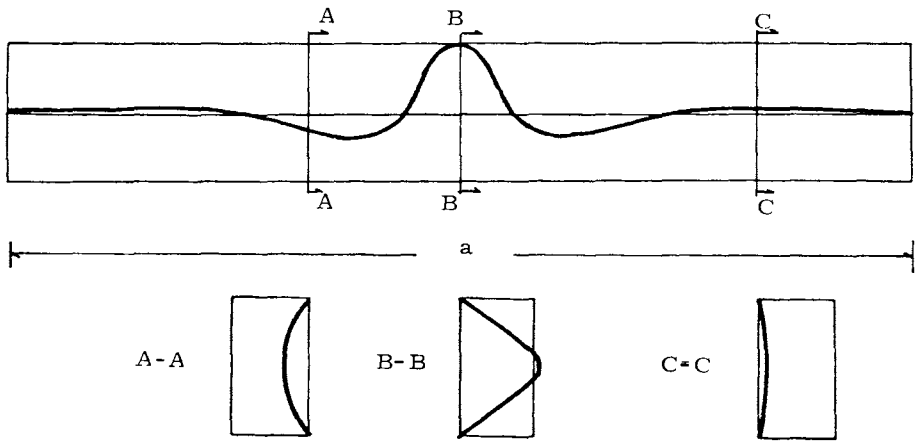

FIG. 11. - BUCKLING MODE FOR COMPRESSION FLANGE (S.S. ALONG y = 0, b) OF BOX BEAM UNDER CASE 2 LOADING , a/b = 6

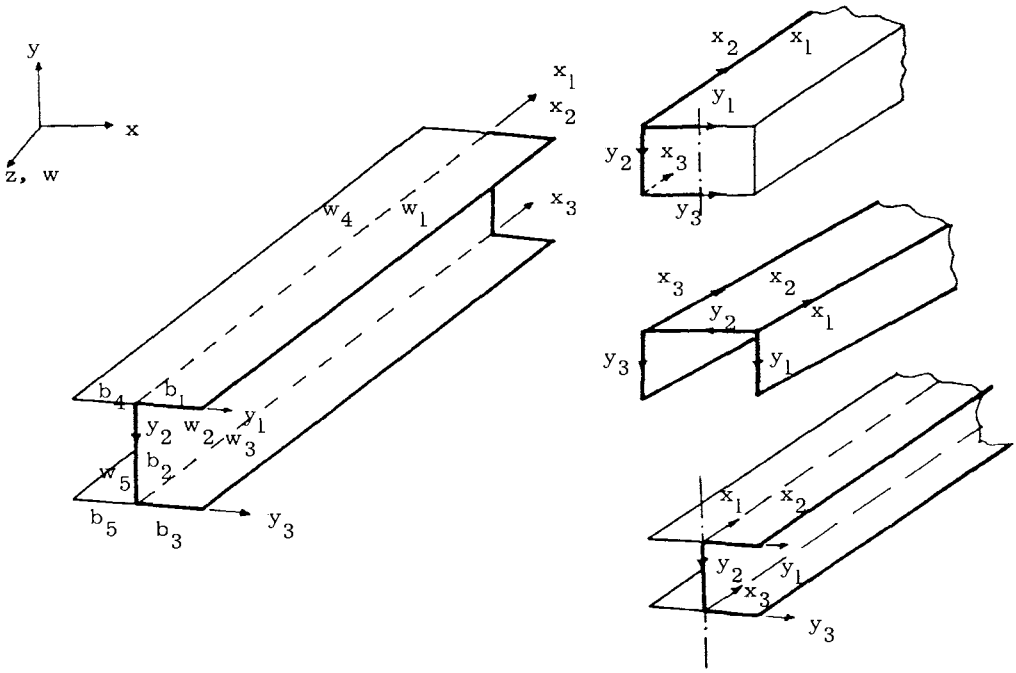

FIG. 12. - TYPICAL CROSS-SECTIONS

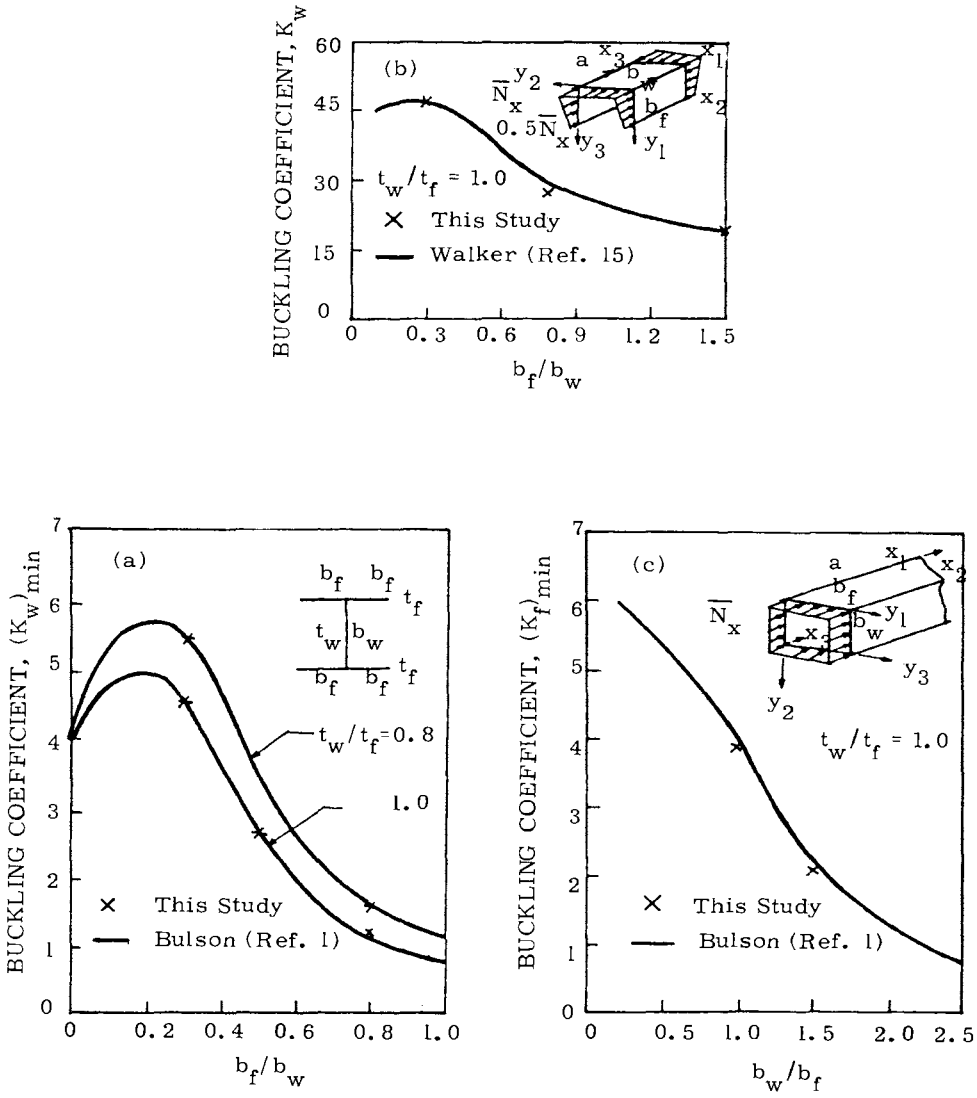

FIG. 13. - COMPARISON OF SOLUTIONS - BUCKLING OF SECTIONS

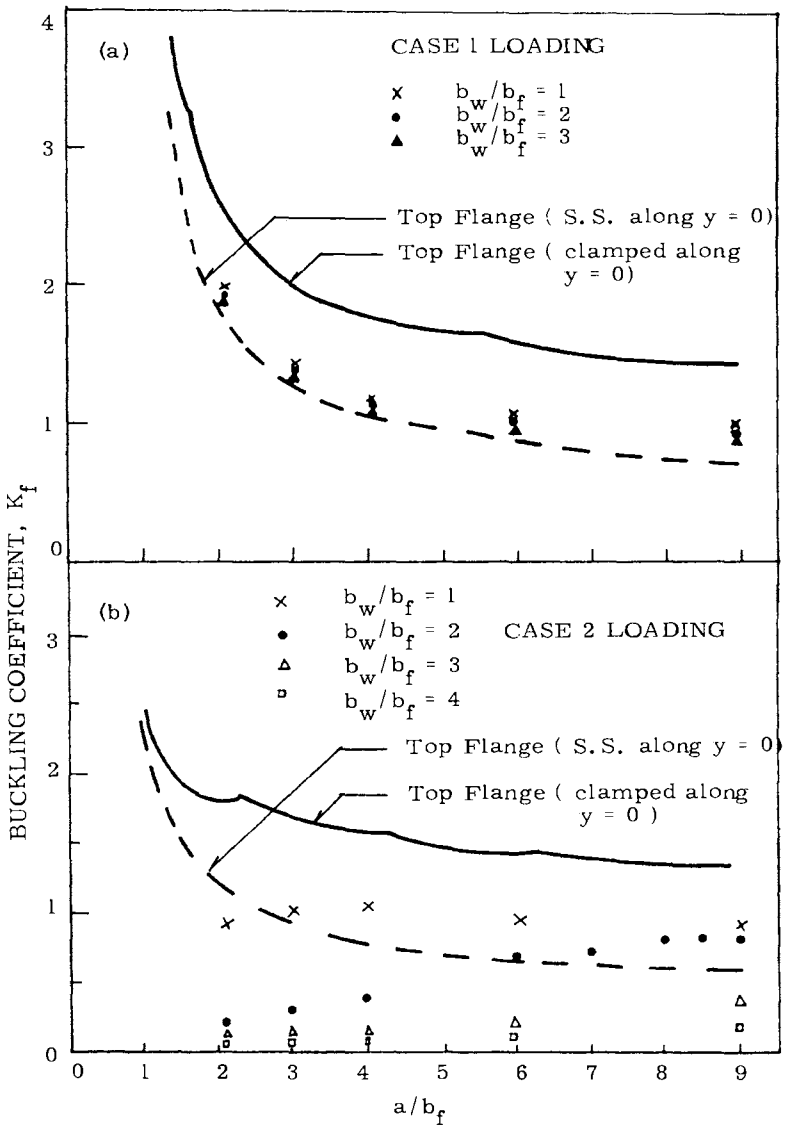

FIG. 14. - BUCKLING COEFFICIENTS OF WIDE-FLANGE BEAMS (t_w/t_f = 1.0)

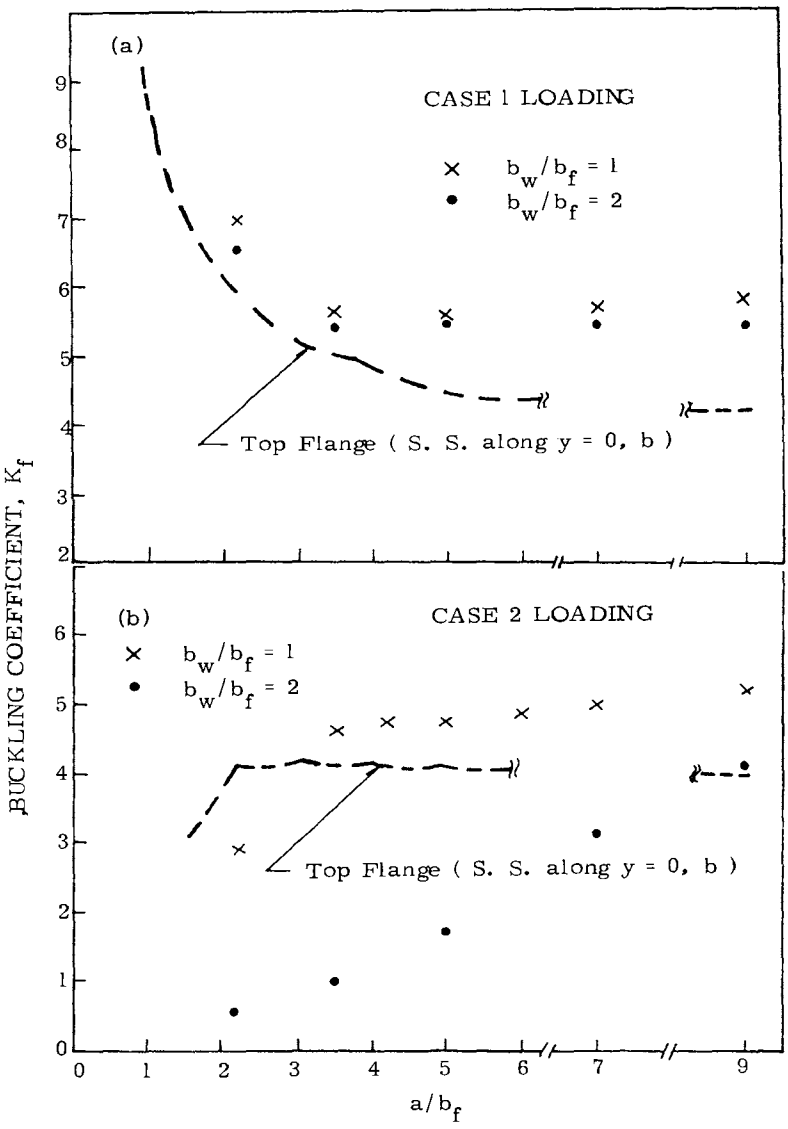

FIG. 15. - BUCKLING COEFFICIENTS OF BOX BEAMS ($t_w/t_f = 1.0$)